A Mathematically Accurate Angular Regression Model Optimizes Phase Activation and Yields Additional Physiological Information in FMRI

John C. Bodenschatz, Daniel B. Rowe

Department of Mathematical and Statistical Sciences, Marquette University, 1313 W. Wisconsin Avenue, Milwaukee, 53233, WI, USA

Abstract

In functional magnetic resonance imaging (fMRI), it is important to observe the functioning brain as fast as possible and at as high of a spatial resolution as possible. Increased spatial and temporal speed results in voxels with increased noise relative to signal and contrast. There is much evidence to suggest that there is important biological information contained within the phase component of the fMRI signal. When the signal-to-noise ratio within a voxel is low, as when there is ultra-high resolution, the marginal statistical distribution of the phase is non-standard and difficult to work with. This non-standard marginal phase distribution at high signal-to-noise ratios is Normally distributed, but at low signal-to-noise ratios needs to be utilized for accurate modeling. In this work, phase-only activation will be computed directly from Lathi's mathematically correct non-Normal distribution, yielding additional physiological information to what is typically observed.

Keywords: FMRI, MLE, phase, activation

1. Introduction

In functional magnetic resonance imaging (fMRI), images are most often collected via single shot echo planar imaging (EPI)— "single shot" meaning only one radio frequency (RF) excitation is applied per measured k-space array. The most commonly used pulse sequence used in EPI is gradient recalled echo (GRE) (Kumar et al., 1975; Bernstein et al., 2004). In general, a given signal equation yields a complex-valued signal s received at a given point (k_x, k_y) in k-space. The steady state GRE signal equation is given by

$$s(k_x, k_y) = \int_{-\infty}^{\infty} \int_{-\infty}^{\infty} \frac{M_0 \sin(\alpha)}{(1 - \cos(\alpha) e^{-TR/T_1})} \times \left(1 - e^{-\mathrm{TR}/T_1}\right) e^{-t/T_2^*} e^{i\gamma \Delta B t} e^{-i2\pi(k_x x + k_y y)} \, dx \, dy, \tag{1}$$

where proton spin density $M_0(x, y)$, longitudinal relaxation time $T_1(x, y)$, observed transverse relaxation time $T_2^*(x, y)$, and $\Delta B(x, y)$ are functions of voxels (x, y) within the physical object being imaged and $t(k_x, k_y)$ is the time at which the point (k_x, k_y) in k-space is scanned (Hargreaves, 2012; Wang et al., 2020). The simplification of replacing $t(k_x, k_y)$ with echo time TE is often used and is equivalent to assuming that all data are acquire at the TE. The repetition time TR is the time between successive RF pulses of the same slice, or equivalently the time between successive measured k-space arrays of the same slice. The flip angle α is commonly set to 90°, which simplifies the quotient term in Equation 1 to M_0.

A point of interest in the signal equation in Equation 1 is the term $e^{i\gamma \Delta B t}$ where ΔB is a catch-all term for any spatio-temporal inhomogeneity in the magnetic field local to a voxel. These fluctuations from the intended uniform

magnetic field can also be caused by scanner imperfections, gradient coil imperfections and eddy currents, patients' own magnetization, tissue composition and interfaces with air, and more (Bernstein et al., 2004; Haacke, 1999; Holland et al., 2010). Since the exponential term that includes ΔB is the only non-Fourier term that includes an imaginary part, the biological information contained within ΔB can be found within the phase of reconstructed images. If the machine were able to perfectly construct a uniform field B_0, eliminating the exponential term $e^{i\gamma\Delta Bt}$, the imaginary part of reconstructed images would be randomly distributed noise resulting in an uninteresting phase image. It is often the case that the true complex-valued nature of fMRI data is ignored, and only magnitude images are studied.

In fMRI, the blood-oxygen-level-dependent (BOLD) signal is interrogated to determine regions of activation (Ogawa et al., 1990). The BOLD signal is a measure of localized brain blood volume and oxygenation changes which are correlates for neuronal activity. These changes occur as a result of certain stimuli or tasks, e.g., right-hand finger tapping, that activate known regions of the brain. The BOLD signal presents itself as a T_2^* effect since the change in magnetic properties of oxygenated and deoxygenated hemoglobin in blood causes a perturbation in the local magnetic field, ΔB, which causes a transverse dephasing of spins. Hence, fMRI time series are T_2^*-weighted images, highlighting regions of the brain with significant T_2^* effects. It is known that

$$1/T_2^* = 1/T_2 + 1/T_2' \tag{2}$$

where T_2 is the "true" transverse relaxation effect due to intrinsic molecular interactions, and T_2' is transverse relaxation due to magnetic field inhomogeneities ΔB. In fact, $1/T_2' = \gamma\Delta B$, matching the previously mentioned

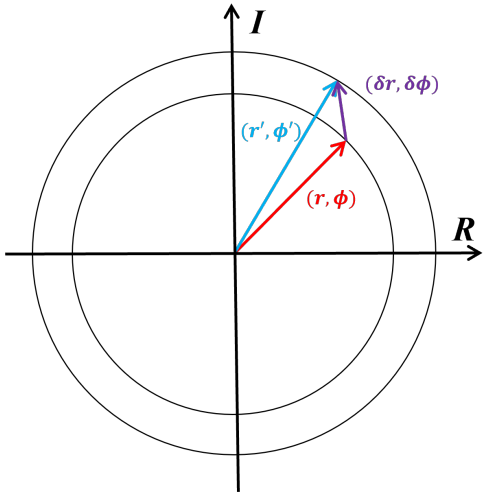

Figure 1: Possible signal changes for a voxel as a results of task-related activation. In red is the baseline signal (r, ϕ), in blue is the task-active signal (r', ϕ'), and in purple is the task-related signal change $(\delta r, \delta \phi)$.

complex exponential term in Equation 1 (Chavhan et al., 2009). The BOLD signal has a measurable effect in both the magnitude (from the term e^{-t/T_2^*}) and phase (from the term $e^{i\gamma \Delta B t}$) of the signal within a voxel. Traditionally the BOLD signal is analyzed in magnitude-only images, discarding any information contained within the phase. Figure 1 depicts the complex plane in which a voxel measurement exists. In red is the baseline signal (r, ϕ), in blue is the task-active signal influenced by BOLD effects (r', ϕ'), and in purple is the task-related signal change $(\delta r, \delta \phi)$. It is possible that there is change in one or both of the magnitude and phase (Rowe, 2005a). If the phase data is ignored, only changes in magnitude can be detected, which leads to the loss of physiological information found in the phase.

Historically in fMRI, a general linear model with Normally distributed errors was used for the marginal distribution of the magnitude component of the time series (Bandettini et al., 1993). However, the Normal assumption is not valid at low signal-to-noise ratios (SNRs). Recently, efforts have been made to use the proper Ricean marginal distribution for the magnitude component in fMRI (Rowe, 2005b; Adrian et al., 2013, 2025). It should be noted that there is also a line of research utilizing the full complex-valued time series (Lai and Glover, 1997; Nan and Nowak, 1999; Rowe and Logan, 2004; Rowe, 2005a). In this line of research, task related magnitude, phase, or magnitude and phase activation is computed within the full complex-valued time series. Ever increasing relaxation of the assumed model parameters was made (Adrian et al., 2018, 2025) as well as Bayesian inference (Yu et al., 2018; Wang et al., 2024, 2025). There has been some effort to estimate and perform inferences on the phase component of the time series (Rowe et al., 2007). Historically researchers centered each voxel time series, unwrapped it, and simply fit a linear regression model with normally distributed errors. However this can have challenges when there is a phase transition on the $[-\pi, \pi]$ boundary and the incorrect distribution is used. In this work, we will use Lathi's mathematically correct phase distribution to compute task-related phase activation (Lathi, 1983).

2. Methods

2.1. Distributions

It has been well established that that MRI voxel values are complex-valued consisting of real and imaginary parts. This is supported by the

fact that images are reconstructed by the inverse Fourier transform of non-Hermitian k-space arrays. The real y_R and imaginary y_I parts of a given voxel value at a specified time contains additive independent and identically distributed Normal noise, $y_R \sim N(\rho\cos\theta, \sigma^2)$ and $y_I \sim N(\rho\sin\theta, \sigma^2)$ (den Dekker and Sijbers, 2005; Gudbjartsson and Patz, 1995; Rowe, 2023). Here, ρ and θ represent the true magnitude and phase signal within the voxel. Thus, the joint distribution of the real and imaginary parts can be expressed as a bivariate Normal distribution with phase-coupled means

$$\begin{aligned} f(y_R, y_I|\rho, \theta, \sigma^2) = &\frac{1}{(2\pi\sigma^2)^{1/2}} \exp\left[-\frac{(y_R - \rho\cos(\theta))^2}{2\sigma^2}\right] \times \\ &\frac{1}{(2\pi\sigma^2)^{1/2}} \exp\left[-\frac{(y_I - \rho\sin(\theta))^2}{2\sigma^2}\right]. \end{aligned} \tag{3}$$

A transformation of variables from the Cartesian random variables (y_R, y_I) to the polar random variables (r, ϕ) can be performed, where $y_R = r\cos\phi$, $y_I = r\sin\phi$ and the Jacobian is found to be $J = r$. This results in the following joint distribution for measured magnitude and phase r and ϕ

$$f(r, \phi|\rho, \theta, \sigma^2) = \frac{r}{2\pi\sigma^2} \exp\left[-\frac{1}{2\sigma^2}\left[r^2 + \rho^2 - 2r\rho\cos(\phi - \theta)\right]\right]. \tag{4}$$

From this bivariate distribution, the Ricean marginal distribution for magnitude with location ρ and scale σ can be integrated out

$$f(r|\rho, \sigma^2) = \frac{r}{\sigma^2} \exp\left[-\frac{r^2 + \rho^2}{2\sigma^2}\right] I_0\left(\frac{r\rho}{\sigma^2}\right) \tag{5}$$

where I_0 is the zeroth order modified Bessel function of the first kind (Rice, 1944; Gudbjartsson and Patz, 1995; Rowe and Logan, 2004). The unnamed non-Normal marginal distribution (which will further be referred

to as the "Lathi" distribution) for phase is found to be

$$f(\phi|\rho,\theta,\sigma^2) = \frac{1}{2\pi}\exp\left[-\frac{\rho^2}{2\sigma^2}\right] \times \left[1+\frac{\rho}{\sigma}\sqrt{2\pi}\cos(\phi-\theta)\exp\left[\frac{\rho^2\cos^2(\phi-\theta)}{2\sigma^2}\right]\Phi\left(\frac{\rho\cos(\phi-\theta)}{\sigma}\right)\right], \tag{6}$$

where $\Phi(x)$ is the cumulative distribution function of the standard Normal distribution (Lathi, 1983; Rowe and Logan, 2004; Rowe and Bodenschatz, 2025). This Lathi distribution is often approximated to be the Normal distribution. A visual comparison of the two distributions is presented in Figure A.1 in Appendix A. This approximation is only good in voxels where the true signal ρ is high relative to the noise σ^2. In regions where $\rho \approx 0$, the Lathi distribution becomes uniform on the interval $[-\pi, \pi]$. A power analysis of the distribution in Equation 6 compared to the Normal approximation is explored in Appendix A.

2.2. Estimation

In fMRI, there is a time series of n measurements collected at each voxel location. An association measure between the time series and the expected response from the fMRI experiment is computed, usually in the form of a linear regression that is applied to only the magnitude of the complex-valued time series. Without task, the parameters in Equation 5 can be estimated via maximum likelihood estimation. The likelihood function is given by

$$L(\rho,\sigma^2) = \prod_{t=1}^{n} f(r_t|\rho,\sigma^2), \tag{7}$$

which upon insertion of the Rice distribution becomes

$$L(\rho,\sigma^2) = \prod_{t=1}^{n} \frac{r_t}{\sigma^2}\exp\left[-\frac{r_t^2+\rho^2}{2\sigma^2}\right] I_0\left(\frac{r_t\rho}{\sigma^2}\right). \tag{8}$$

Similarly, without task, the parameters in Equation 6 can be estimated via maximum likelihood estimation. The likelihood function is given by

$$L(\rho, \theta_0, \sigma^2) = \prod_{t=1}^{n} f(\phi_t|\rho, \theta_0, \sigma^2), \tag{9}$$

with $\theta_t = \theta_0$ where θ_0 is the baseline phase. In the case where task is present, the likelihood function is updated to become

$$L(\rho, \theta_0, \theta_1, \sigma^2) = \prod_{t=1}^{n} f(\phi_t|\rho, \theta_0, \theta_1\sigma^2), \tag{10}$$

with $\theta_t = \theta_0 + \theta_1 x_t$ where θ_1 is the additive task-related signal and $x_t \in \{0, 1\}$ is an indicator of expected response at time t.

The likelihood for the null and alternative hypotheses can be maximized and the parameters estimated via maximum likelihood estimation. This can be done with a multitude of optimization methods. We choose to equivalently minimize the negative log likelihood function using MATLAB's "fmincon" function which employs a sequential quadratic programming method (The MathWorks Inc., 2022). Since it is well known that the task-related magnitude signal change is extremely small compared to the baseline, an aggregated magnitude MLE $\hat{\rho}$ is estimated using MATLAB's "mle" function and used when computing the phase MLEs from Equations 9 and 10. This also provides an estimate for $\hat{\sigma}^2$ which is updated during the phase estimation. Utilizing the distribution in Equation 6 for each of the n observations at time t, the phase likelihood becomes

$$\begin{aligned} L(\theta_0, \theta_1, \sigma^2) = \prod_{t=1}^{n} \left\{ \frac{1}{2\pi} \exp\left(-\frac{\hat{\rho}^2}{2\sigma^2}\right) \left[1 + \right.\right. \\ \left.\left. \frac{\hat{\rho}}{\sigma}\sqrt{2\pi}\cos(\phi_t - \theta_t) \exp\left(\frac{\hat{\rho}^2\cos^2(\phi_t - \theta_t)}{2\sigma^2}\right) \Phi\left(\frac{\hat{\rho}\cos(\phi_t - \theta_t)}{\sigma}\right) \right] \right\} \end{aligned} \tag{11}$$

where $\theta_t = \theta_0$ under the null hypothesis and $\theta_t = \theta_0 + \theta_1 x_t$ under the alternative hypothesis. An alternative method of maximization (the simple grid search) and it's experimental results are further discussed in Appendix B.

A voxel-wise likelihood ratio statistic $\lambda = L_{H_0}/L_{H_1}$ can be computed as the ratio of the null likelihood over the alternative likelihood, and the $\Lambda = -2\ln(\lambda) \sim \chi^2(1)$ test statistic formed (Wilks, 1938). Since there is a single degree of freedom, a z-statistic can be formed

$$z = \text{sign}(\hat{\theta}_1)\sqrt{-2\ln(\lambda)} \tag{12}$$

and utilized to detect "task-active" voxels (Severini, 2000).

3. Results

3.1. Simulated Results

This method was tested on both simulated and experimental fMRI data. The simulated data was made using the same MR parameters as the experimental data for consistency of methods and comparability of results. The simulated fMRI time series data was generated using SHAKER v1.1 (Bodenschatz and Rowe, 2025). The simulated time series is of slice 91 from a size 128 phantom in the Axial plane. The MRI parameters were set to be the following: Acceleration Factor = 1, Field Strength = 3 T, TE = 50 ms, TR = 1000 ms, Flip Angle = 90°, EESP = 0.832 ms, and Number of Coils = 1. The data was simulated with the Gradient Echo signal equation (Equation 1) using a Cartesian k-space trajectory. The experimental design involved an initial 16 rest images followed by 19 epochs, each consisting of 16 task images followed by 16 rest images, for a total of 624 images. The initial 3

images are discarded for analysis. The SNR was set to 5 and the CNR was set to 0.25. There were 6 degrees of phase added to the region of activation.

Figure 2 are voxel-wise estimates that do not use the Lathi distribution in Equation 6. Figures 2a and 2b depict the MLE estimates for magnitude and variance from Equation 8. Figure 2c shows the signal-to-noise ratio (SNR) defined by $SNR = \hat{\rho}/\hat{\sigma}$, which was intentionally simulated to be about 5. Figure 2d depicts the mean angular phase $\bar{\phi}$ of the time series. Figures 2e and 2f are the simple linear regression coefficient estimates for baseline phase θ_0 and task-related phase θ_1. The baseline phase coefficient estimate appears reasonable within the brain when compared to the mean angular phase, but poorly estimates the regions in empty space. Similarly, the task related phase coefficient estimate is very unreasonable in empty space, and within the brain there is a very clear banding artifact that comes from the phase wraparound near the $[-\pi, \pi]$ boundary. This artifact makes it impossible to determine with confidence the existence of task-related phase change.

Figure 3 shows the maximum likelihood estimates of $\hat{\theta}_0$, $\hat{\sigma}^2$, and $\hat{\theta}_1$ under the null and alternative hypothesis in the top and bottom rows respectively. Contrary to Figure 2, these estimations are based on the more accurate Lathi distribution in Equation 6 and formed via the maximum likelihood presented in Equation 11. In the top row, Figures 3a and 3b depict the estimates $\hat{\theta}_0$ and $\hat{\sigma}^2$ under the null hypothesis that $\theta_t = \theta_0$. In the bottom row, Figures 3d, 3e, and 3f depict the estimates $\hat{\theta}_0$, $\hat{\theta}_1$, and $\hat{\sigma}^2$ under the alternative hypothesis that $\theta_t = \theta_0 + \theta_1 x_t$. The estimate $\hat{\theta}_0$ is approximately the same for both hypotheses while the estimate for $\hat{\sigma}^2$ appears to be slightly scaled back in empty space under the alternative hypothesis. The estimate for $\hat{\theta}_1$ looks

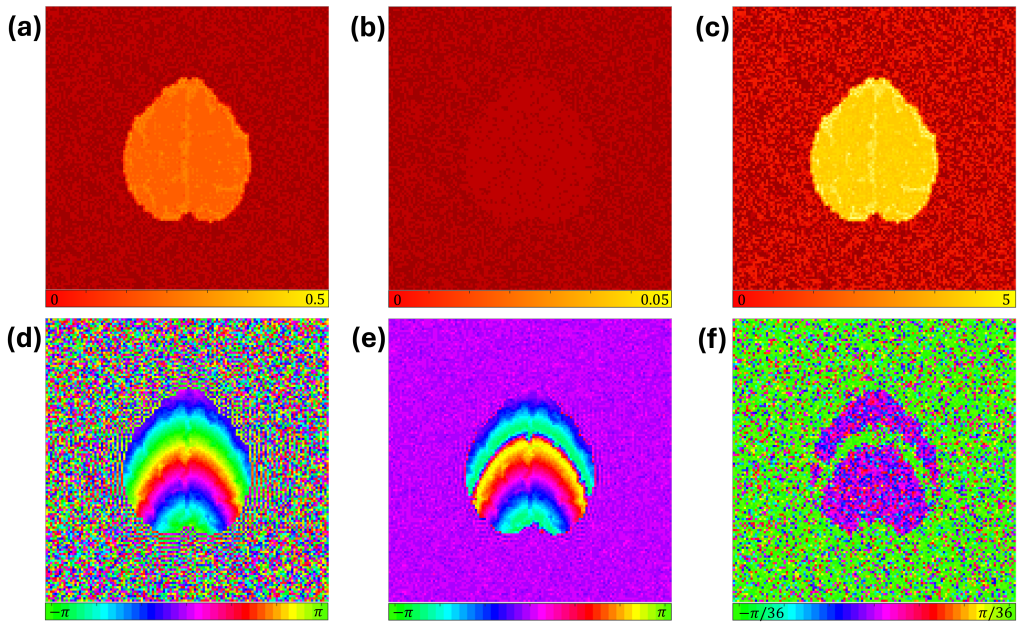

Figure 2: Maximum likelihood estimation for $\hat{\rho}$ (a) and $\hat{\sigma}^2$ (b) from Equation 8 with resulting SNR (c). Average measured voxel phase $\bar{\phi}$ (d). Linear regression estimate for $\hat{\theta}_0$ (e) and $\hat{\theta}_1$ (f). Notice the banding effect in (f) that is a result of phase wrap-around. This can make diagnosing regions that contain task-related activity difficult.

nearly uniform at about 0 inside the brain, and noisy in empty space.

While the volume image of $\hat{\theta}_1$ in Figure 3 appears fairly smooth in Figure 3e, closer examination reveals details about the nature of θ_1. Calculating the likelihood ratio statistic as described in Section 2.2 and corresponding z-statistic as described by Equation 12, we can highlight exactly where the task-related phase coefficient θ_1 is significant. The z-statistics produced from this method, presented in Figure 4, are filtered using the Benjamini-Hochberg procedure to control the false discovery rate at the $\alpha = 0.05$ level which

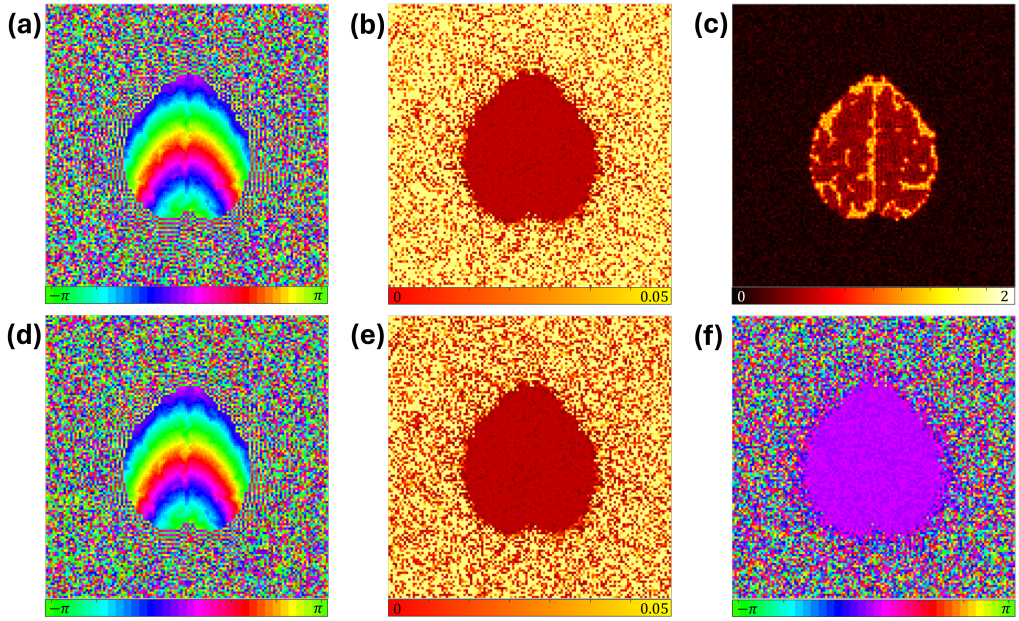

Figure 3: Maximum likelihood estimations for $\hat{\theta}_0$ (a) and $\hat{\sigma}^2$ (b) under the null hypothesis, $\theta_t = \theta_0$ with anatomical image (c). Maximum likelihood estimations for $\hat{\theta}_0$ (d), $\hat{\sigma}^2$ (e), and $\hat{\theta}_1$ (f) under the alternative hypothesis, $\theta_t = \theta_0 + \theta_1 x_t$.

resulted in a critical z-statistic of 4.45 (Benjamini and Hochberg, 2018). The zoomed in region indicates the left motor cortex, the region that is expected to have a task-related signal change as a result of right-hand finger tapping (the performed task for the experimental data). Here we can clearly identify a region of task-related phase change. The average value for $\hat{\theta}_1$ in the voxels that were simulated to have an additional 6 degrees of task-related phase change was found to be 5.34 degrees.

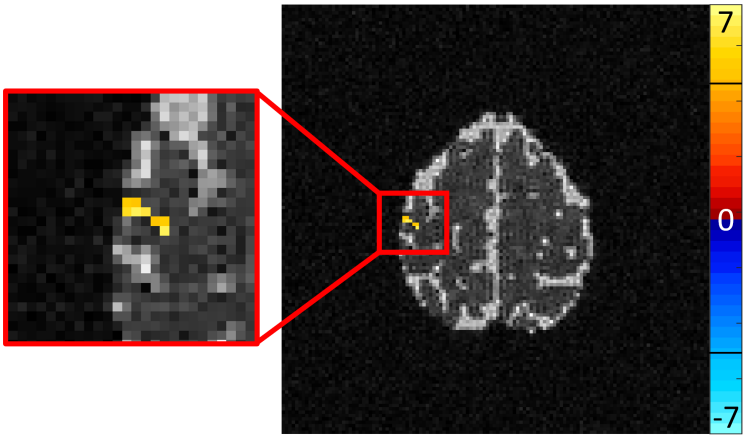

Figure 4: Z-statistics from the likelihood ratio test statistic described in Equation 12, filtered by the Benjamini–Hochberg procedure controlling the false discovery rate at the $\alpha = 0.05$ level. The critical z-statistic was found to be 4.45, as indicated by the black lines on the color bar. The left motor cortex is enhanced to the left. This is the region of expected activation for right hand finger tapping experiments.

3.2. Experimental Results

Experimental data is from a block design right-hand finger tapping experiment on a 3.0-Tesla General Electric Signa LX MRI scanner. The imaging parameters were n_z=7 slices of 2.5 mm thick and 128×128 array size with a field-of-view FOV=24.0 cm, echo time TE=60.4 ms, effective echo spacing EESP=0.832 ms, and time-of-repetition TR=1 s. The experiment timing followed an initial 16 s of rest followed by 19 epochs of 16 s of task alternating with 16 s of rest resulting in a total of n_t=624 total image volumes. The initial 3 images are discarded for analysis. Each slice image at each time point, was Nyquist ghost corrected (Nencka et al., 2009). Images were phase

drift corrected by subtracting each voxel's angular phase temporal mean. A local second order polynomial was spatially fit to the resultant difference of each phase image in the time-series. The spatially fitted phase is angularly subtracted from the original time series (Sakitis and Rowe, 2025). A simple linear regression model was fit to each voxel's unwrapped phase time series and angularly subtracted off. Then the angular mean was added to each voxel's time series, resulting in a linearly stable phase over time.

Figure 5 are voxel-wise estimates that do not use the Lathi distribution in Equation 6; this figure is the experimental equivalent to Figure 2. Figures 5a and 5b depict the MLE estimates for magnitude and variance from Equation 8. In both of these figures some Nyquist ghosting artifacts are present, particularly in the region above the brain. Figure 5c shows the signal-to-noise ratio (SNR) which was found to be about 5 within the brain. These brain images were collected using a body receive coil with decreased SNR, resulting in particularly noisy data. Figure 5d depicts the mean angular phase $\bar{\phi}$ of the experimental time series. Figures 5e and 5f are the simple linear regression coefficient estimates for baseline phase θ_0 and task-related phase θ_1. Similar to the simulated data, the baseline phase coefficient estimate appears reasonable within the brain when compared to the mean angular phase, but poorly estimates the regions in empty space. Also the task related phase coefficient estimate is very unreasonable in empty space, and within the brain there is a very clear banding artifact that comes from the phase wraparound near the $[-\pi, \pi]$ boundary. This artifact makes it impossible to determine with confidence the existence of task-related phase change.

Figure 6 shows the maximum likelihood estimates of $\hat{\theta}_0$, $\hat{\sigma}^2$, and $\hat{\theta}_1$ under

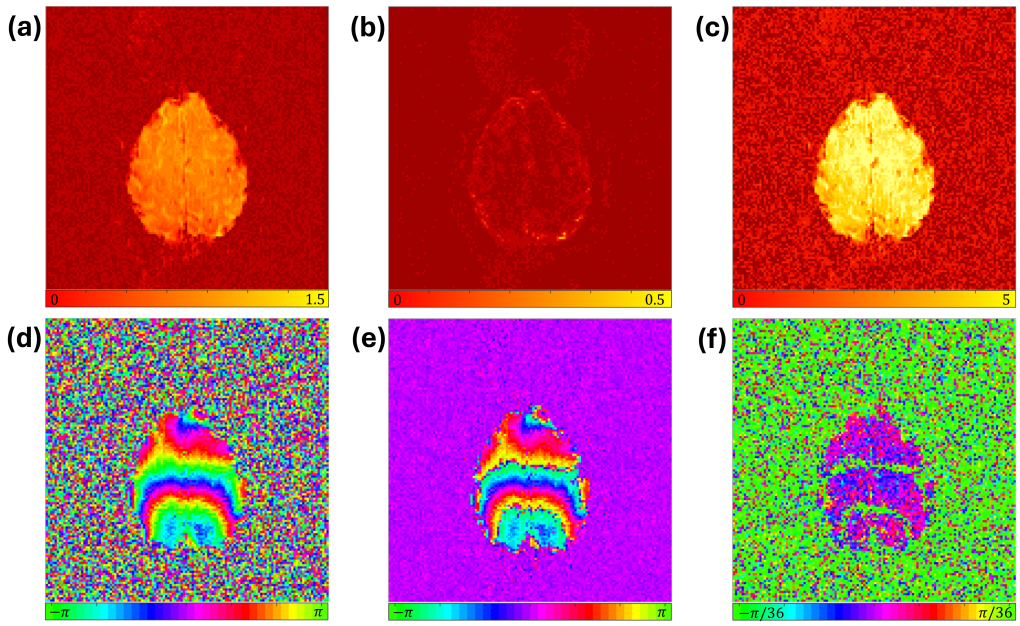

Figure 5: Maximum likelihood estimation for $\hat{\rho}$ (a) and $\hat{\sigma}^2$ (b) from Equation 8 with resulting SNR (c). Average measured voxel phase $\bar{\phi}$ (d). Linear regression estimate for $\hat{\theta}_0$ (e) and $\hat{\theta}_1$ (f). Notice the banding effect in (f) that is a result of phase wrap-around. This can make diagnosing regions that contain task-related activity difficult.

the null and alternative hypothesis in the top and bottom rows respectively; this is the experimental equivalent of Figure 3. In the top row, Figures 6a and 6b depict the estimates $\hat{\theta}_0$ and $\hat{\sigma}^2$ under the null hypothesis that $\theta_t = \theta_0$. In the bottom row, Figures 6d, 6e, and 6f depict the estimates $\hat{\theta}_0$, $\hat{\theta}_1$, and $\hat{\sigma}^2$ under the alternative hypothesis that $\theta_t = \theta_0 + \theta_1 x_t$. The estimate $\hat{\theta}_0$ is approximately the same for both hypotheses while the estimate for $\hat{\sigma}^2$ appears to be slightly scaled back in empty space under the alternative hypothesis. The estimate for $\hat{\theta}_1$ looks mostly uniform at about 0 inside the brain and

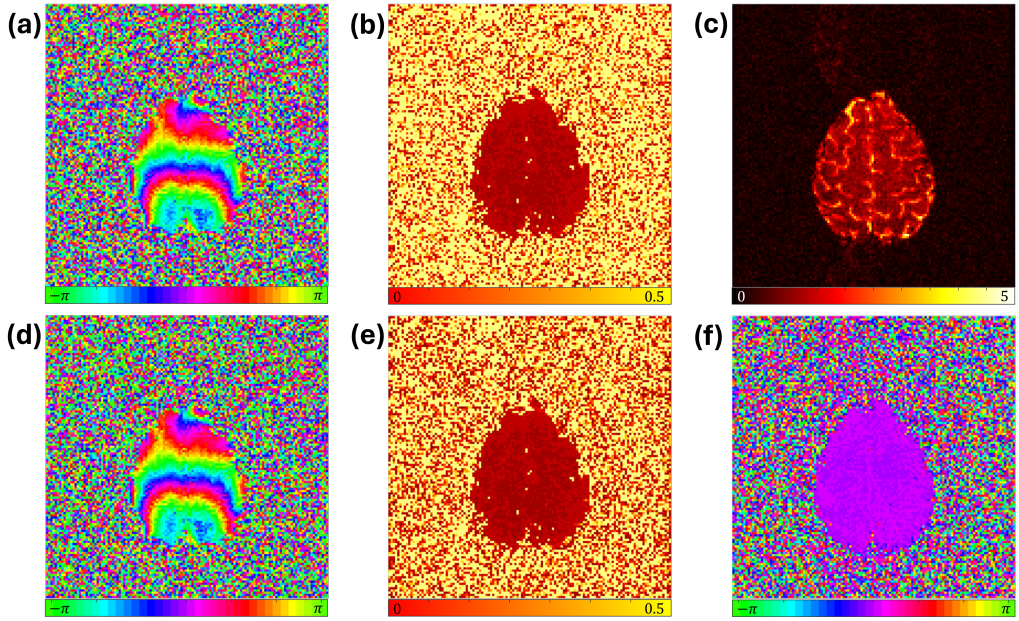

Figure 6: Maximum likelihood estimations for $\hat{\theta}_0$ (a) and $\hat{\sigma}^2$ (b) under the null hypothesis, $\theta_t = \theta_0$ with anatomical image (c). Maximum likelihood estimations for $\hat{\theta}_0$ (d), $\hat{\sigma}^2$ (e), and $\hat{\theta}_1$ (f) under the alternative hypothesis, $\theta_t = \theta_0 + \theta_1 x_t$.

noisy in empty space, as one might expect.

The z-statistics produced from the method described in Section 2.2, presented in Figure 7, are filtered using the Benjamini-Hochberg procedure to control the false discovery rate at the $\alpha = 0.05$ level which resulted in a critical z-statistic of 3.89 The zoomed in region indicates the left motor cortex, the region that is expected to have a task-related signal change as a result of right-hand finger tapping (the performed task for the experimental data). There is a distinct region of voxels that have task-related phase increase. The average value for $\hat{\theta}_1$ in the voxels that were determined to have task-related

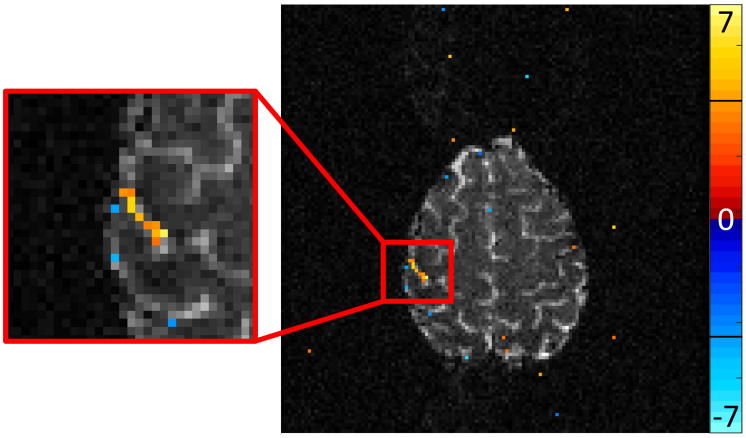

Figure 7: Z-statistics from the likelihood ratio test statistic described in Equation 12, filtered by the Benjamini–Hochberg procedure controlling the false discovery rate at the $\alpha = 0.05$ level. The critical z-statistic was found to be 3.89, as indicated by the black lines on the color bar. The left motor cortex is enhanced to the left. This is the region of expected activation for right hand finger tapping experiments.

phase change was found to be 6.33 degrees.

4. Discussion

It is rarely the case in fMRI studies that the whole complex-valued data is studied, leaving out the phase information to look only at the magnitude data. Further, when phase data *is* analyzed, the time series distribution of measurements is often simplified to the Normal distribution, which is only valid in voxels with high SNR. In this work the non-Normal distribution from Lathi, which is valid for all SNRs was used to estimate task-related changes in the phase signal. This maximum likelihood estimation model

was tested on simulated data and promising results were demonstrated on complex-valued experimental data. In both the simulated and experimental data it was demonstrated that the non-Normal Lathi distribution works well at all SNRs and has detected task-related phase changes in the left motor cortex from unilateral a right-handed finder tapping experiment. This work shows exciting results for the ability to detect additional biological information contained in the phase. This motivates further investigations into phase activation resulting from local magnetic field changes due to vascularity or even direct neuronal current (Mullinger et al., 2014; Harris et al., 2011; Shmuel and Leopold, 2008).

CRediT authorship contribution statement

John C. Bodenschatz: Writing - original draft, Visualization, Software, Investigation, Formal analysis. **Daniel B. Rowe:** Writing - review & editing, Supervision, Resources, Project administration, Methodology, Formal analysis, Conceptualization.

Declaration of competing interest

None declared.

Appendix A. Power analysis of alternative distributions

In the hypothesis test described in Section 2 a significance level of $\alpha = 0.05$ was chosen. This represents the probability of committing a Type I error or false positive, which in this application would mean falsely claiming a voxel has some task-related phase change when in reality it does not. A

result of fixing $\alpha = 0.05$ is the value of the power β of the hypothesis test. Statistical power is the ability of a hypothesis test to correctly reject the null hypothesis when it is false, or for this application, the probability of correctly identifying a voxel as having some task-related phase change. A depiction of statistical power is shown in Figure A.1. In this figure, the maximum likelihood estimates of the parameters from an experimental voxel that was determined to be task-active are used to draw theoretical distributions. In black is the distribution for phase measurements under the null hypothesis that $\theta_t = \theta_0$. In red and blue are the distributions for $\theta_0 + \theta_1$ under the alternative hypothesis that $\theta_t = \theta_0 + \theta_1 x_t$ using the Lathi assumption and Normal approximation, respectively. The power is represented by the similarly colored area under each $\theta_0 + \theta_1$ distribution curve, to the right of the critical value $\theta_{0\alpha}$. Here we can visually see that the Lathi distribution (red) has larger statistical power than the Normal assumption (blue) due to the large difference in area to the right of the critical value.

The example in Figure A.1 is for a specific voxel with an estimated value for θ_0 and $\theta_0 + \theta_1$. One way to generalize to other voxels is to vary the effect size (i.e. compare different values of θ_1) and observe how the power changes. This was done without loss of generality by using the estimate for θ_0 from the same voxel that was used for the previous example and adjusting the estimate for θ_1 from 0 to 1 radian. The power for each effect size is then calculated and plotted, resulting in Figure A.2. The red and blue power curves are for the alternative hypothesis following a Lathi and Normal distribution respectively. For effect sizes where $\theta_1 \lessapprox 0.5$ radians (about 30 degrees), the Lathi distribution provides higher statistical power. The max-

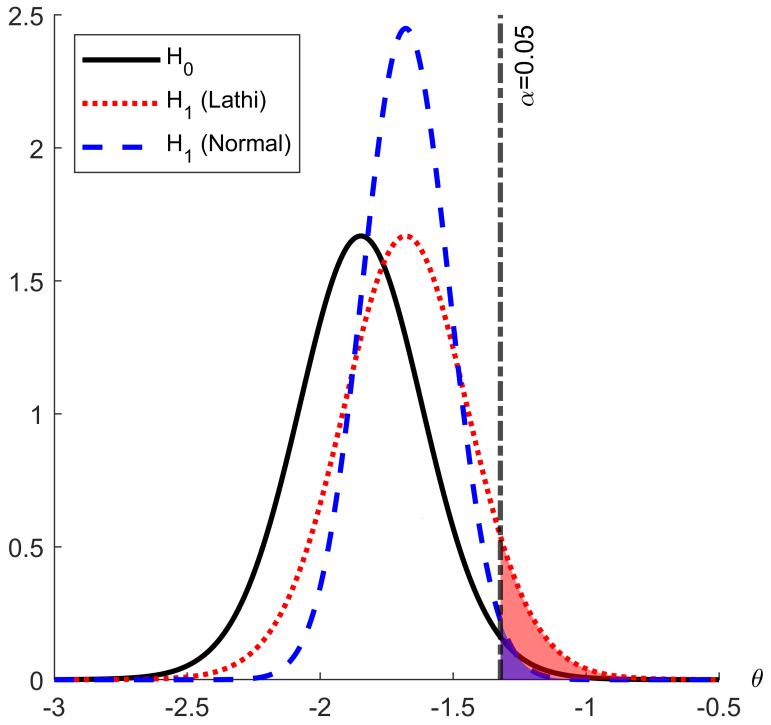

Figure A.1: Theoretical distributions based on maximum likelihood estimates from an active voxel in Figure 7. The null hypothesis (black) assumes the Lathi distribution in Equation 6. The alternative hypothesis using the Lathi (red) and Normal (blue) distributions. The power is the highlighted area to the right of the critical value for each alternative hypothesis distribution.

imum likelihood estimate for θ_1 for the voxel from the active experimental voxel is marked by a vertical line at about 0.18. Measurements for θ_1 are largely at or below this level.

Note that this demonstrative example is for a one-tailed hypothesis test which assumes the phase change will be positive. The methods described in Section 2 support a two-tailed test, which is what is measured in practice

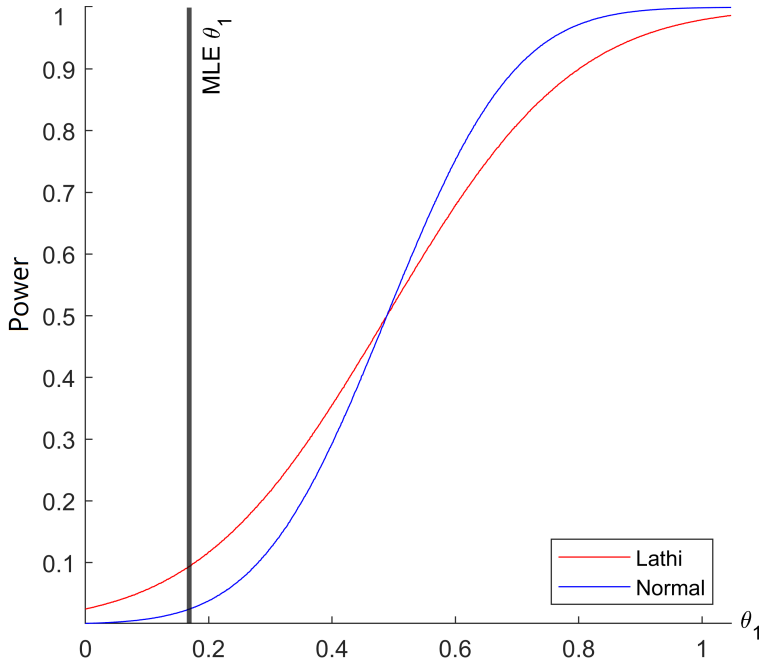

Figure A.2: Power curves for Lathi (red) and Normal (blue) alternative hypotheses under a null hypothesis that assumes the Lathi distribution in Equation 6. The vertical line at about 0.18 indicates where the maximum likelihood estimate $\hat{\theta}_1$ was located for this particular active voxel.

in Section 3. This allows for the possibility of a negative change in phase, though it is observed that most changes are in the positive direction.

Appendix B. Grid search approach to parameter estimation

To validate the results produced from the maximum likelihood estimation, a simple grid search was performed to estimate the parameters θ_0, θ_1, and σ^2 for the null and alternative hypothesis. Search boundaries were tightened using prior knowledge of what the values for $\hat{\theta}_0$, $\hat{\theta}_1$, and $\hat{\sigma}^2$ were expected to

be. The search interval for the baseline phase was $\hat{\theta}_0 \in [\bar{\phi} - \pi/24, \bar{\phi} + \pi/24]$, which assumes that the estimate $\hat{\theta}_0$ should be reasonably close to the mean value $\bar{\phi}$. The search interval for the additive phase was $\hat{\theta}_1 \in [-\pi/72, \pi/24]$ which assumes that the task-related phase change in a voxel is relatively small and likely positive. Lastly, the search interval for the variance was set to $\hat{\sigma}^2 \in [\hat{\sigma}^2 - \hat{\sigma}^2/5, \hat{\sigma}^2 + \hat{\sigma}^2/5]$ which assumes that the variance is reasonably close to the previously estimated variance $\hat{\sigma}^2$ from the magnitude estimation as described in Section 2.2. Each interval had 10 linearly spaced search points, resulting in 100 possible combinations of $\hat{\theta}_0$, $\hat{\theta}_1$, and $\hat{\sigma}^2$ for the null hypothesis and 1,000 possible combinations for the alternative hypothesis. This is a very low precision grid search; best practice would involve a significantly denser search space. However, this small search took 3 hours to run on the same computer that computed the maximum likelihood estimates in less than 3 minutes.

Figure B.1 shows the estimated parameters $\hat{\theta}_0$, $\hat{\theta}_1$, and $\hat{\sigma}^2$ under the null and alternative hypothesis in the top and bottom rows respectively. The baseline phase estimate $\hat{\theta}_0$ and variance estimate $\hat{\sigma}^2$ are comparable across the hypotheses. An interesting contrast between the grid search result for variance $\hat{\sigma}^2$ and $\hat{\theta}_1$ to the maximum likelihood result is the regions in space. While the estimations within the brain are similar, the grid search tends to estimate values near zero in space whereas the maximum likelihood estimates are much noisier across the domain.

The z-statistics produced from the grid search method, presented in Figure B.2, are similarly filtered using the Benjamini-Hochberg procedure to control the false discovery rate at the $\alpha = 0.05$ level which resulted in a crit-

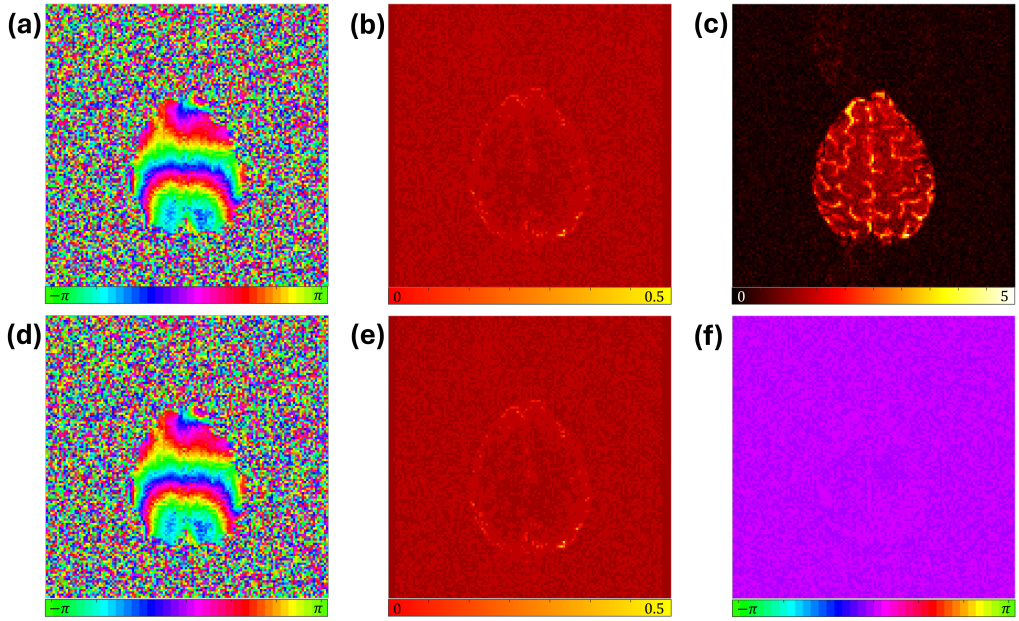

Figure B.1: Grid search results for $\hat{\theta}_0$ (a) and $\hat{\sigma}^2$ (b) under the null hypothesis, $\theta_t = \theta_0$ with anatomical image (c). Grid search results for $\hat{\theta}_0$ (d), $\hat{\sigma}^2$ (e), and $\hat{\theta}_1$ (f) under the alternative hypothesis, $\theta_t = \theta_0 + \theta_1 x_t$.

ical z-statistic of 4.27. The zoomed in region indicates the left motor cortex, the region that is expected to have a task-related signal increase as a result of right-hand finger tapping (the performed task for the experimental data).

When comparing the results from the grid search to the results from the maximum likelihood estimation in Figure 6 some interesting conclusions can be drawn. Perhaps a limitation of the search space, the grid search tends to return a value near 0 for $\hat{\sigma}^2$ and $\hat{\theta}_1$ in empty space whereas the maximum likelihood estimates are randomly distributed as one might expect. The grid search does return approximately the same region of task-related phase

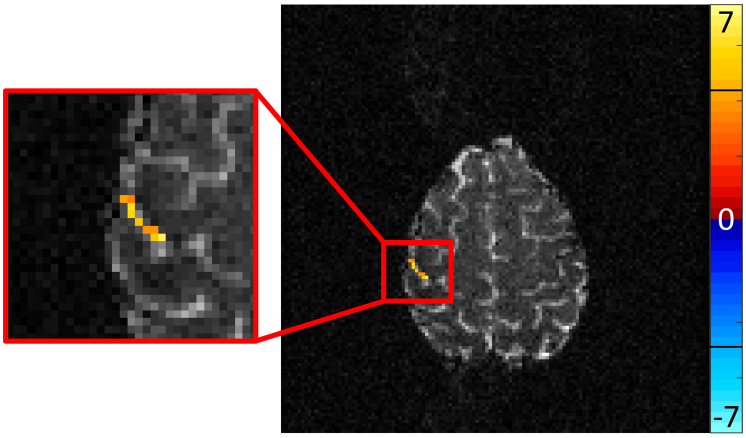

Figure B.2: Z-statistics from the likelihood ratio test statistic described in Equation 12, filtered by the Benjamini–Hochberg procedure controlling the false discovery rate at the $\alpha = 0.05$ level. The critical z-statistic was found to be 4.27, as indicated by the black lines on the color bar. The left motor cortex is enhanced to the left. This is the region of expected activation for right hand finger tapping experiments.

activation as the maximum likelihood estimate in Figure 7 with a slightly higher critical statistic of 4.27, eliminating some noise in the FDR filtered z-statistics (and possibly some task detection as well).

Appendix C. Experimental results for all seven slices

As mentioned in Section 3.2, the experimental data included seven axial slices. A particularly active slice was chosen for model demonstration in that section. Figure C.1 shows a summary of results for all seven slices. The rows are organized by slice; slice 6 was examined in Section 3.2. The first column shows the maximum likelihood estimate for ρ for each slice. There is a small

amount of Nyquist ghosting present in the magnitude estimation for each slice. The second and third columns show the estimates for θ_0 and θ_1 under the alternative hypothesis. Each baseline phase estimate $\hat{\theta}_0$ has some amount of phase wrapping that is known to cause issues when using simple linear estimation. The task-related phase change estimate $\hat{\theta}_1$ is visually similar for each slice when on the $[-\pi, \pi]$ scale. The fourth column is the variance estimation $\hat{\sigma}^2$. The final column are the Benjamini-Hochberg filtered z-statistics superimposed onto anatomical magnitude images of the slices. The task-related phase change in the left motor cortex is most noticeable in slices 6 (critical $z = 3.89$) and 7 (3.88), with trace amounts of activation detected in slices 4 (3.90) and 5 (3.90). Slices 1-4 exhibit no obvious signs of a task-related phase change.

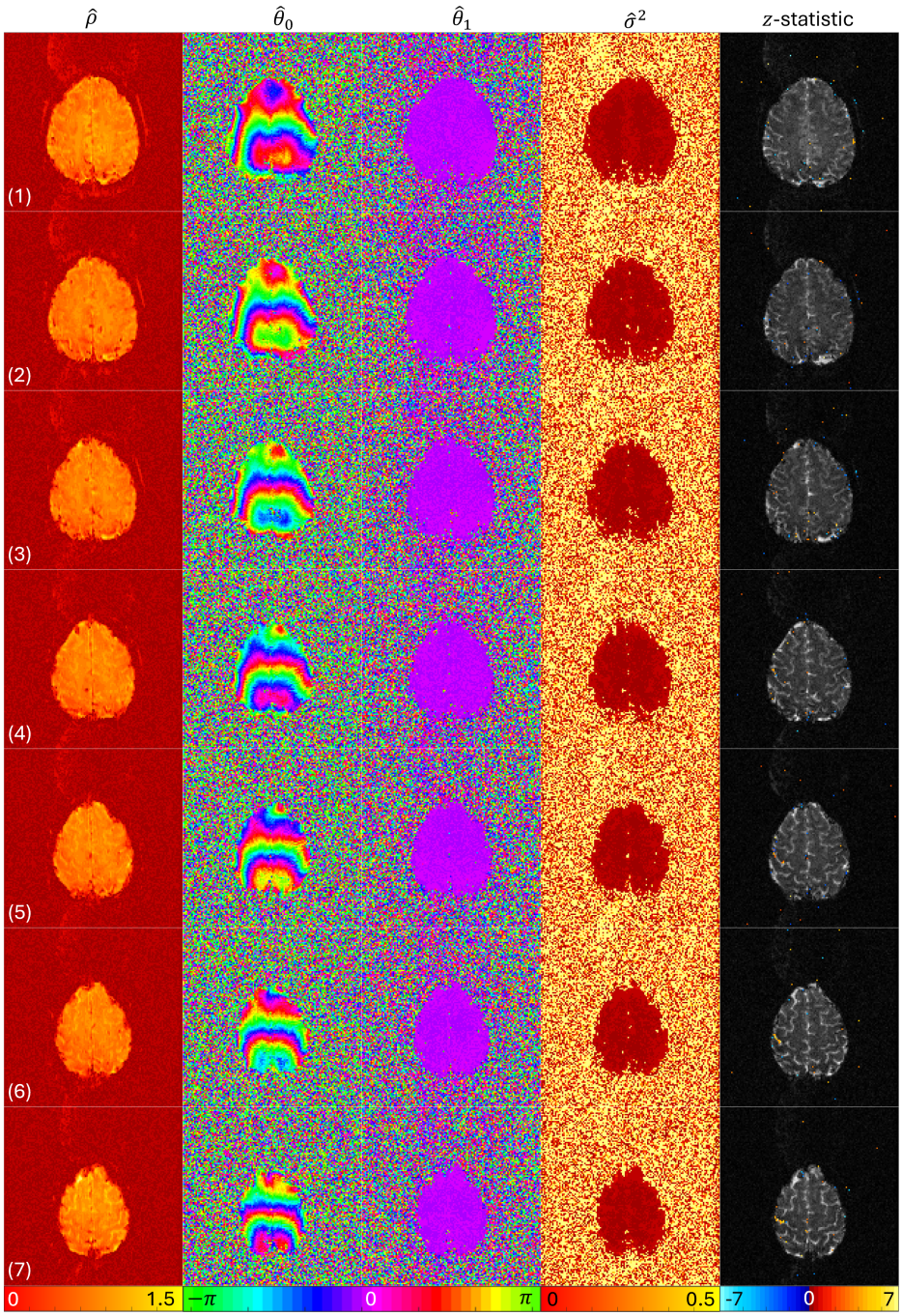

Figure C.1: Summary images for all seven experimental slices (rows). The columns indicate magnitude estimation $\hat{\rho}$, baseline phase $\hat{\theta}_0$, task-related phase change $\hat{\theta}_1$, and variance $\hat{\sigma}^2$ under the alternative hypothesis, and FDR=0.05 filtered z-statistics. Slice 6 was explored further in Section 3.2.

References

Adrian, D.W., Maitra, R., Rowe, D.B., 2013. Ricean over Gaussian modelling in magnitude fMRI Analysis-Added Complexity with Negligible Practical Benefits. Stat 2, 303–316.

Adrian, D.W., Maitra, R., Rowe, D.B., 2018. Complex-Valued Time Series Modeling for Improved Activation Detection in fMRI Studies. The Annals of Applied Statistics 12, 1451–1478.

Adrian, D.W., Maitra, R., Rowe, D.B., 2025. Rice-Distributed Autoregressive Time Series Modeling of Magnitude Functional MRI Data. The Annals of Applied Statistics 19. doi:10.1214/24-AOAS1981.

Bandettini, P.A., Jesmanowicz, A., Wong, E.C., Hyde, J.S., 1993. Processing Strategies for Time-Course Data Sets in Functional MRI of the Human Brain. Magnetic Resonance in Medicine 30, 161–173. doi:https://doi.org/10.1002/mrm.1910300204.

Benjamini, Y., Hochberg, Y., 2018. Controlling the False Discovery Rate: A Practical and Powerful Approach to Multiple Testing. Journal of the Royal Statistical Society: Series B (Methodological) 57, 289–300. doi:10.1111/j.2517-6161.1995.tb02031.x.

Bernstein, M., King, K., Zhou, X., 2004. Handbook of MRI Pulse Sequences. Elsevier Inc. doi:10.1016/B978-0-12-092861-3.X5000-6. publisher Copyright: © 2004 Elsevier Inc. All rights reserved.

Bodenschatz, J.C., Rowe, D.B., 2025. Simulation and Harmonic Analysis of k-Space Readout (SHAKER). URL: https://arxiv.org/abs/2502.17620, arXiv:2502.17620.

Chavhan, G.B., Babyn, P.S., Thomas, B., Shroff, M.M., Haacke, E.M., 2009. Principles, Techniques, and Applications of T_2^*-based MR Imaging and Its Special Applications. RadioGraphics 29, 1433–1449. doi:10.1148/rg.295095034.

den Dekker, A.J., Sijbers, J., 2005. Implications of the Rician Distribution for fMRI Generalized Likelihood Ratio Tests. Magnetic Resonance Imaging 23, 953–959. doi:https://doi.org/10.1016/j.mri.2005.07.008.

Gudbjartsson, H., Patz, S., 1995. The Rician distribution of noisy MRI data. Magnetic Resonance in Medicine 34, 910–914. doi:https://doi.org/10.1002/mrm.1910340618.

Haacke, E.M., 1999. Magnetic Resonance Imaging: Physical Principles and Sequence Design.

Hargreaves, B.A., 2012. Rapid Gradient-Echo Imaging. Journal of Magnetic Resononance Imaging 36, 1300–1313.

Harris, J.J., Reynell, C., Attwell, D., 2011. The Physiology of Developmental Changes in BOLD Functional Imaging Signals. Developmental Cognitive Neuroscience 1, 199–216. doi:https://doi.org/10.1016/j.dcn.2011.04.001.

Holland, D., Kuperman, J.M., Dale, A.M., 2010. Efficient Correction of Inhomogeneous Static Magnetic Field-Induced Dis-

tortion in Echo Planar Imaging. NeuroImage 50, 175–183. doi:https://doi.org/10.1016/j.neuroimage.2009.11.044.

Kumar, A., Welti, D., Ernst, R.R., 1975. NMR Fourier Zeugmatography. Journal of Magnetic Resonance (1969) 18, 69–83. doi:https://doi.org/10.1016/0022-2364(75)90224-3.

Lai, S., Glover, G.H., 1997. Detection of BOLD fMRI Signals Using Complex Data. Proceedings of the International Society for Magnetic Resonance in Medicine 1997, 1671. doi:https://doi.org/10.1002/mrmp.22419970134.

Lathi, B., 1983. Modern Digital and Analog Communication. Oxford University Press.

Mullinger, K., Mayhew, S., Bagshaw, A., Bowtell, R., Francis, S., 2014. Evidence that the Negative BOLD Response is Neuronal in Origin: A Simultaneous EEG–BOLD–CBF Study in Humans. NeuroImage 94, 263–274. doi:https://doi.org/10.1016/j.neuroimage.2014.02.029.

Nan, F.Y., Nowak, R.D., 1999. Generalized Likelihood Ratio Detection for fMRI Using Complex Data. IEEE Transactions on Medical Imaging 18, 320–329.

Nencka, A.S., Hahn, A.D., Rowe, D.B., 2009. A Mathematical Model for Understanding the STatistical effects of k-space (AMMUST-k) Preprocessing on Observed Voxel Measurements in fcMRI and fMRI. Journal of Neuroscience Methods 181, 268–282.

Ogawa, S., Lee, T.M., Kay, A.R., Tank, D.W., 1990. Brain Magnetic Resonance Imaging with Contrast Dependent on Blood Oxygenation. Pro-

ceedings of the National Acadamy of Sciences U. S. A. 87, 9868–9872. doi:https://doi.org/10.1073/pnas.87.24.9868.

Rice, S.O., 1944. Mathematical Analysis of Random Noise. Bell System Technical Journal 23, 282–332. doi:https://doi.org/10.1002/j.1538-7305.1944.tb00874.x.

Rowe, D.B., 2005a. Modeling Both Magnitude and Phase of Complex fMRI Data. NeuroImage 25, 1310–24. doi:10.1016/j.neuroimage.2005.01.034.

Rowe, D.B., 2005b. Parameter Estimation in the Magnitude-Only and Complex-Valued fMRI Data Models. Neuroimage 25, 1124–1132.

Rowe, D.B., 2023. Statistics of Intrinsic FMRI Data. Proceedings of the Joint Statistical Meeting doi:https://doi.org/10.5281/zenodo.10002334.

Rowe, D.B., Bodenschatz, J.C., 2025. Distributionally Accurate FMRI Phase Activation. Proceedings of the Joint Statistical Meeting doi:10.5281/zenodo.16921786.

Rowe, D.B., Logan, B.R., 2004. A Complex Way to Compute fMRI Activation. Neuroimage 23, 1078–1092.

Rowe, D.B., Meller, C.P., Hoffmann, R.G., 2007. Characterizing Phase-Only fMRI Data with an Angular Regression Model. Journal of Neuroscience Methods 161, 331–341.

Sakitis, C.J., Rowe, D.B., 2025. Bayesian Merged Utilization of GRAPPA and SENSE (BMUGS) for In-Plane Accelerated Reconstruction Increases

fMRI Detection Power. Magnetic Resonance Imaging 115, 110252. doi:https://doi.org/10.1016/j.mri.2024.110252.

Severini, T.A., 2000. Likelihood Methods in Statistics. Oxford Statistical Science Series, Oxford University Press, London, England.

Shmuel, A., Leopold, D.A., 2008. Neuronal Correlates of Spontaneous Fluctuations in fMRI Signals in Monkey Visual Cortex: Implications for Functional Connectivity at Rest. Human Brain Mapping 29, 751–761. doi:https://doi.org/10.1002/hbm.20580.

The MathWorks Inc., 2022. MATLAB version: 24.1.0 (R2024a). URL: `https://www.mathworks.com`.

Wang, X., Hernando, D., Reeder, S.B., 2020. Phase-based T_2 Mapping with Gradient Echo Imaging. Magnetic Resonance in Medicine 84, 609–619.

Wang, Z., Rowe, D.B., Li, X., Brown, D.A., 2024. A Fully Bayesian Approach for Comprehensive Mapping of Magnitude and Phase Brain Activation in Complex-Valued fMRI Data. Magnetic Resonance Imaging 109, 271–285. doi:https://doi.org/10.1016/j.mri.2024.03.029.

Wang, Z., Rowe, D.B., Li, X., Brown, D.A., 2025. Efficient Fully Bayesian Approach to Brain Activity Mapping with Complex-Valued fMRI Data. Journal of Applied Statistics 52, 1299–1314. doi:10.1080/02664763.2024.2422392.

Wilks, S.S., 1938. The Large-Sample Distribution of the Likelihood Ratio for Testing Composite Hypotheses. The Annals of Mathematical Statistics 9, 60–62.

Yu, C., Prado, R., Ombao, H., Rowe, D.B., 2018. A Bayesian Variable Selection Approach Yields Improved Detection of Brain Activation From Complex-Valued fMRI. Journal of the American Statistical Association 113, 1395–1410. doi:10.1080/01621459.2018.1476244.